THE JOURNAL OF PHYSICAL CHEMISTRY C

Article

pubs.acs.org/JPCC

Manipulation of Surface Plasmon Resonance in Sub-Stoichiometry Molybdenum Oxide Nanodots through Charge Carrier Control Technique

Yiwen Li,[†,‡] Jiaji Cheng,[§] Yizun Liu,[†] Peizhao Liu,[∥] Wanqiang Cao,[∥] Tingchao He,[*,⊥] Rui Chen,[*,†] and Zikang Tang[*,‡]

[†]Department of Electrical and Electronic Engineering, South University of Science and Technology of China, Shenzhen, 518055, People's Republic of China

[‡]The Institute of Applied Physics and Materials Engineering, University of Macau, Avenida da Universidade, Taipa, Macau, People's Republic of China

[§]Institut de Chimie de la Matière Condensée de Bordeaux CNRS - UPR 9048, Pessac, 33608, France

[∥]School of Materials Science and Engineering, Hubei University, Wuhan, 430062, People's Republic of China

[⊥]College of Physics and Energy, Shenzhen University, Shenzhen 518060, People's Republic of China

Supporting Information

ABSTRACT: Semiconductor nanocrystals are intriguing because they show surface plasmon absorption features like noble metallic nanoparticles. In contrast with metal, manipulation of their unique plasmonic resonance could be easily realized by the free-carrier concentration. Here, it is demonstrated that MoO_{3-x} nanodots can exhibit striking surface plasmon resonance located at near-infrared region under treatment of two different reducing agents. Furthermore, the tunable resonance mode has been achieved through appropriate redox processes. Refractive index sensing has been demonstrated by monitoring the plasmonic peak. The improved sensing application is ascribed to the enhanced electric field in the plasmonic nanocrystals. These new insights into MoO_{3-x} nanodots pave a way to develop novel plasmonic applications such as photothermal therapy, light harvesting, and sensing.

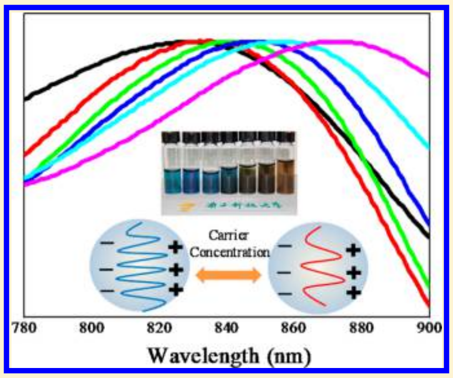

1. INTRODUCTION

Surface plasmon resonances (SPR) have been investigated over a few decades because of their promising potential applications for sensing refractive index of surrounding medium,[1] enhanced emitting,[2] enhanced light scattering,[3] and so forth. Currently, the main candidates for plasmonic materials are noble metallic nanoparticles, especially gold and silver which possess appropriate dielectric behavior and unique weak damping parameters. However, their expensive cost and surfactant-assisted preparation remain challenges for their future developments.[4,5] Recently, a series of new plasmonic material candidates have emerged, for example, the substoichiometry semiconductor nanocrystals such as $Cu_{2-x}S$. These kinds of materials are actually heavily doped semiconductors. Their carrier concentrations can be controlled through redox reaction and thus exhibit strong plasmonic resonance between 1500 and 2000 nm.[6,7] Compared with metallic nanoparticles, the advantages of semiconductor nanocrystals can be attributed to their facile tunability for optical response. It is well-known that the extinction peak is fixed for metallic materials once their synthesis is completed because the SPR frequency is only a function of size, shape, and composition. In contrast, carrier concentration of semiconductor can be easily controlled through chemical doping.[8−10] The plasmonic resonance frequency is closely related to the doping level according to the Drude−Lorentz model:

$$\omega_p = \sqrt{\frac{ne^2}{\varepsilon_0 m_e}} \tag{1}$$

where ω_p is the bulk plasmon frequency, which is proportional to the square root of free-carrier concentration (n). On the basis of this equation, one can see that the plasmonic energy is very sensitive to the doping levels. Besides $Cu_{2-x}S$, researchers have also found other metal-free doped semiconductor counterparts showing similar SPR features in the infrared region, including indium oxide,[11] germanium telluride,[12] tungsten oxide,[13] zinc oxide,[14,15] and so forth. Their dynamically controlled SPR response was also realized through the investigation of defect engineering[16,17] and liquid exfoliation approach.[18] However, their optical resonance is located in the near-infrared (NIR) spectra region, and few studies have been reported focusing on the optical region below 1 μm, which has higher spectrum

Received: November 2, 2016
Revised: February 14, 2017
Published: February 15, 2017

DOI: 10.1021/acs.jpcc.6b11047
J. Phys. Chem. C 2017, 121, 5208−5214

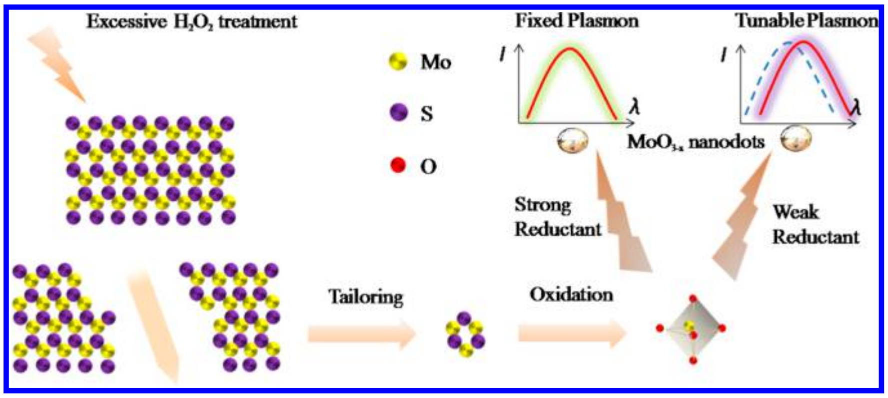

Figure 1. Schematic procedures demonstrate the MoO_{3-x} nanodots prepared from MoS_2 nanosheets during oxidation and reduction process.

overlap with real solar radiation.[19] Besides, expensive metal elements such as indium limit their practical application. Another counterpart semiconductor is transition-metal oxides (TMO), which exhibit unique SPR properties because of their outer-d valence electrons. Recently, as a conventional TMO, molybdenum oxides have demonstrated fascinating plasmonic behavior after different treatments such as solar light radiation (photochemical reduction),[20] shape transformation (chemical doping),[21] and noble metal or polymer hybrids[22,23] toward their significant application such as gas sensors.[24] However, tunability of carrier densities through chemical doping redox to manipulate SPR performance is still absent.

Hence, in this work, high stability molybdenum oxide nanodots have been designed and synthesized from chemical oxidation of bulk molybdenum disulfide (MoS_2) and subsequently have formed substoichiometry MoO_{3-x} with different reducing agents, including sodium borohydride ($NaBH_4$) and ascorbic acid (AA). These MoO_{3-x} colloidal materials have shown strong NIR SPR features around 700−1000 nm. The transition-metal valence states and defect properties under different reducing agents have been analyzed. The dynamic tunability of their charge carrier concentration could be conducted by facile redox chemical doping process, and a weaker reductant AA has been found to successfully obtain scalable tunability of SPR through controlling the reducing concentration. The carrier-dependent strategy sheds light on low-cost glass coating for infrared switching device application, such as smart window,[25,26] which usually utilizes indium oxide or zinc oxide films as electrochromic materials to control NIR transmittance. Moreover, this kind of control may contribute to the development of plasmonic nanocrystal tailored for wider applications such as photothermal therapy,[27] light harvesting,[28,29] and sensing.[30]

2. EXPERIMENTAL SECTION

Preparation of Pristine MoO_3 Nanodots Aqueous Solution. Typically, 20 mg MoS_2 powder was dispersed in 20 mL mixed solution containing 18.5 mL DI water and 1.5 mL H_2O_2 (30 wt % aqueous solution). The dispersion was stirred at room temperature overnight in a 25 mL glass vial. The mixed solution turned from black to shallow yellow color because of oxidation accompanied by spontaneous exfoliation. The as-prepared dispersion was then applied for MoO_3 general characterization and subsequent reduction procedures.

Preparation of Substoichiometry MoO_{3-x} Nanodots. The as-prepared aqueous solution of MoO_3 nanodots was utilized for the precursor to produce substoichiometry MoO_{3-x}. The removal of excess H_2O_2 is necessary before the reaction because reductant such as $NaBH_4$ would react with H_2O_2 in aqueous solution. We employed heating treatment to remove H_2O_2 in solution under 60−70 °C for about 30−60 min until bubbles were not observed. We applied two different reductants to prepare MoO_{3-x} nanodots. One is as-prepared $NaBH_4$ solution, with various amounts with molar ratio of Na:Mo from 0.2 to 8. The component turned from light yellow to green or blue immediately after shaking or sonication according to different reductant concentrations. The other reductant is ascorbic acid (AA). In this case, higher concentrations were used because of its much weaker reducing ability compared with $NaBH_4$. Finally, the various AA powders were added into yellow pristine MoO_3 nanodot solution to prepare MoO_{3-x} aqueous samples under various molar ratios of AA:Mo from 6 to 136. The component turned from yellow to blue after shaking or sonication immediately.

Characterization. The morphologies of MoO_3 and MoO_{3-x} nanodots were characterized by high-resolution transmission electron microscopy (HRTEM) with a JEM-ARM 200F microscope operating at 200 kV. The size distribution was conducted by Gaussian fitting. Chemical analysis carried out by scanning transmission electron microscopy (STEM) coupled with energy-dispersive X-ray spectroscopy (EDX) was acquired with a JEOL 2200FS equipped with a field emissive gun, operating at 200 kV. X-ray photoelectron spectroscopy (XPS) was utilized to identify the stoichiometry of MoO_{3-x} nanodots. Different samples were dropped onto silicon substrates before XPS measurements. The deconvolution method was employed by Lorentz fitting. UV−vis extinction tests were performed by a UV−vis spectrometer (Dual-FL, Horiba).

3. RESULTS AND DISCUSSION

The schematic procedures are described in Figure 1. Substoichiometry MoO_{3-x} nanodots were obtained through reduction of molybdenum oxides. MoO_3 nanodots were prepared by spontaneous exfoliation as well as by tailoring of bulk MoS_2 flakes in aqueous solution. The procedures can be found elsewhere.[31] Briefly, MoS_2 powders were dispersed in water with adding appropriate H_2O_2 for oxidation. The color of the mixture would turn from light yellow overnight to produce MoO_3 nanodots because H_2O_2 could tailor and decrease the size of MoS_2 flakes. The chemical reaction is indicated by the following equation:

$$MoS_2 + 9H_2O_2 \rightarrow MoO_3 + 7H_2O + 2H_2SO_4 \quad (2)$$

Detailed preparation procedures and characterizations of MoO_3 nanodots are described in the Experimental Section. The TEM

DOI: 10.1021/acs.jpcc.6b11047
J. Phys. Chem. C 2017, 121, 5208−5214

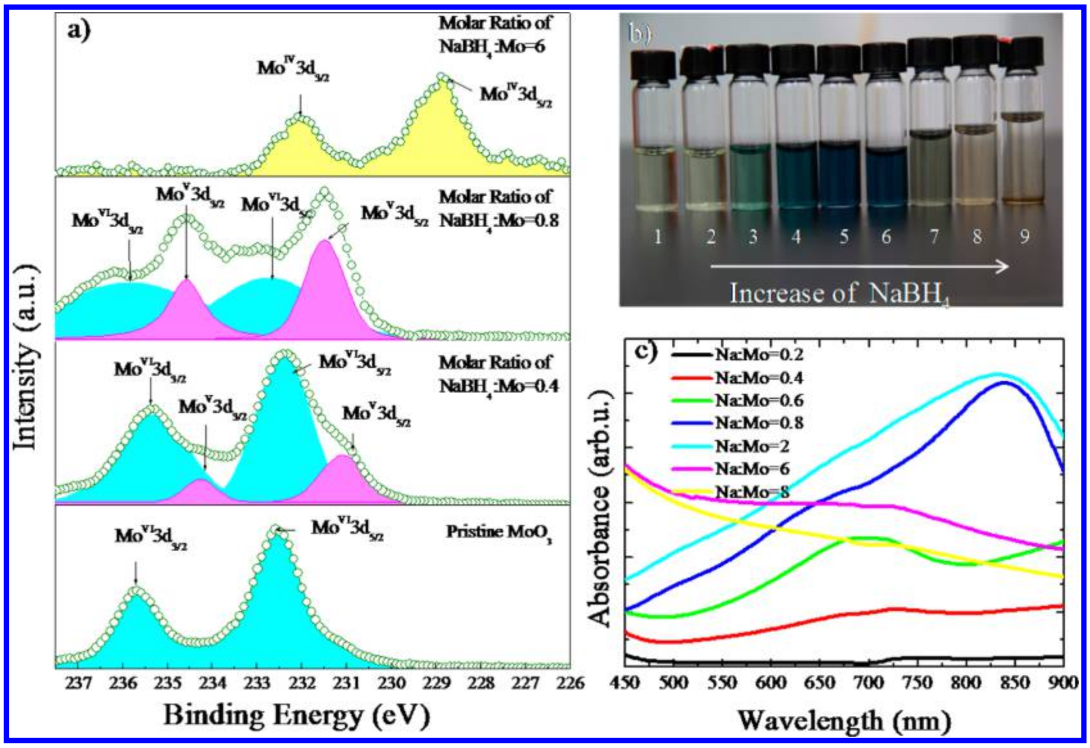

Figure 2. (a) XPS spectra of Mo 3d in pristine MoO_3 and substoichiometry MoO_{3-x} under various $NaBH_4$ concentration reductions. (b) Photography of MoO_{3-x} nanodot aqueous solution under various molar ratios of $NaBH_4$: Mo (0, 0.2, 0.4, 0.6, 0.8, 2, 6, 8, 10) corresponding to No. 1−9 samples, respectively. (c) UV−vis absorption spectra of MoO_{3-x} nanodots with different $NaBH_4$ concentrations corresponding to samples No. 2−8.

image of the sample is shown in Figure S1a, where monodisperse nanodots with size of 10.1 ± 1.2 nm can be clearly seen. Figure S1b is high-resolution TEM characterization (HRTEM), which demonstrates that the 0.18 nm spacing in lattice fringes of pristine molybdenum oxide nanodots corresponds to the (002) plane of α-MoO_3. Moreover, the selective area electron diffraction pattern (SAED), which is shown in the insert of Figure S1b, demonstrates the (211) and (130) planes of α-MoO_3. The extinction cross section is mainly dependent on absorption, which is translated from electron−electron surface scattering, but the scattering cross section can be ignored in the case of small particle size according to Mie theory.[30] No apparent plasmonic feature could be observed in pristine MoO_3. However, when reducing agents are conducted to react with as-prepared MoO_3 nanodots, their optical absorption exhibits evident variance.

First, sodium borohydride ($NaBH_4$), a conventional reductant for metallic nanoparticles, was utilized to reduce as-prepared MoO_3 nanodots. Different concentrations of $NaBH_4$ solutions were added into the TMO suspension. Figure 2b shows the color change of the solutions with reductant amount, labeled from No. 1 to No. 9. The aqueous solution of pristine MoO_3 suspension (No. 1) exhibits the same color as that with a molar ratio of Na:Mo = 0.2 (No. 2). With a continuous increase of $NaBH_4$ to archive the molar ratio to 0.4 and 0.6 (No. 3 and No. 4), the solution turns green. For the subsequent extent reduction, the sample shows blue color with 0.8 and 2 molar ratio loading (No. 5 and No. 6) and brown color with 6, 8, and 10 molar ratio loading (No. 7−9), respectively. These results indicate that there are various reductive valence states in the molybdenum oxides to form substoichiometry semiconductor compounds. All the samples exhibit high stability without any aggregation except No. 9. To better understand the reasons why molybdenum valence state transformation induced color change, the element chemical valence characterizations were used to analyze various molybdenum oxide valences with different $NaBH_4$ concentrations. The XPS spectra of Mo 3d are shown in Figure 2a. For the pristine MoO_3 sample (No. 1) derived from H_2O_2, two peaks located at around 235.68 and 232.58 eV were detected. The two doublets correspond to binding energies of $3d_{3/2}$ and $3d_{5/2}$ of molybdenum, respectively, which are in agreement with the feature peak modes of Mo(VI) in the typical α-MoO_3. With the treatment of $NaBH_4$ reductant, the peaks down-shift to lower binding energies, as a result of appearance of Mo(V) oxidation state in the reducing products. For the sample No. 3 with molar ratio of 0.4, the intensity of Mo(V) peaks at 234.58 and 231.48 eV increases clearly compared to that of Mo(VI) peaks. By deconvolution and calculation of the relative peak intensity values, the ratio of Mo(VI) to Mo(V) turns out to be 3.71, which the percentage of Mo(V) in Mo is inferred as 21%, that is, a substoichiometry nanodot of $MoO_{2.89}$. With the continuous reduction by increasing the reductant amount, the No. 5 with 0.8 molar ratio shows stronger intensity of Mo(V) peaks both for $3d_{3/2}$ and for $3d_{5/2}$. The ratio of Mo(VI) to Mo(V) drops to 0.78, corresponding to 56% Mo(V) in Mo content, and the approximate substoichiometry oxides refer to $MoO_{2.71}$. The obvious increase of Mo(V) (magenta areas) and decrease of Mo(VI) (light cyan areas) could be found in Figure 2a. For the No. 7 sample under a larger amount of $NaBH_4$ reduction, the XPS shows apparent peaks of Mo(IV) at around 232.08 and 229.08 eV for $3d_{3/2}$ and $3d_{5/2}$, which indicates the strong reduction from Mo(VI) to Mo(IV) under an excessive amount of $NaBH_4$. The corresponding elemental analysis of No. 3 sample was performed by using EDX coupled to STEM as shown in Figure S2. The existence of Mo is confirmed in the mapping which relates to the nanodots observed in the STEM image. Furthermore, the EDX mapping of Na exhibits that the sites of molybdenum oxide

DOI: 10.1021/acs.jpcc.6b11047
J. Phys. Chem. C 2017, 121, 5208−5214

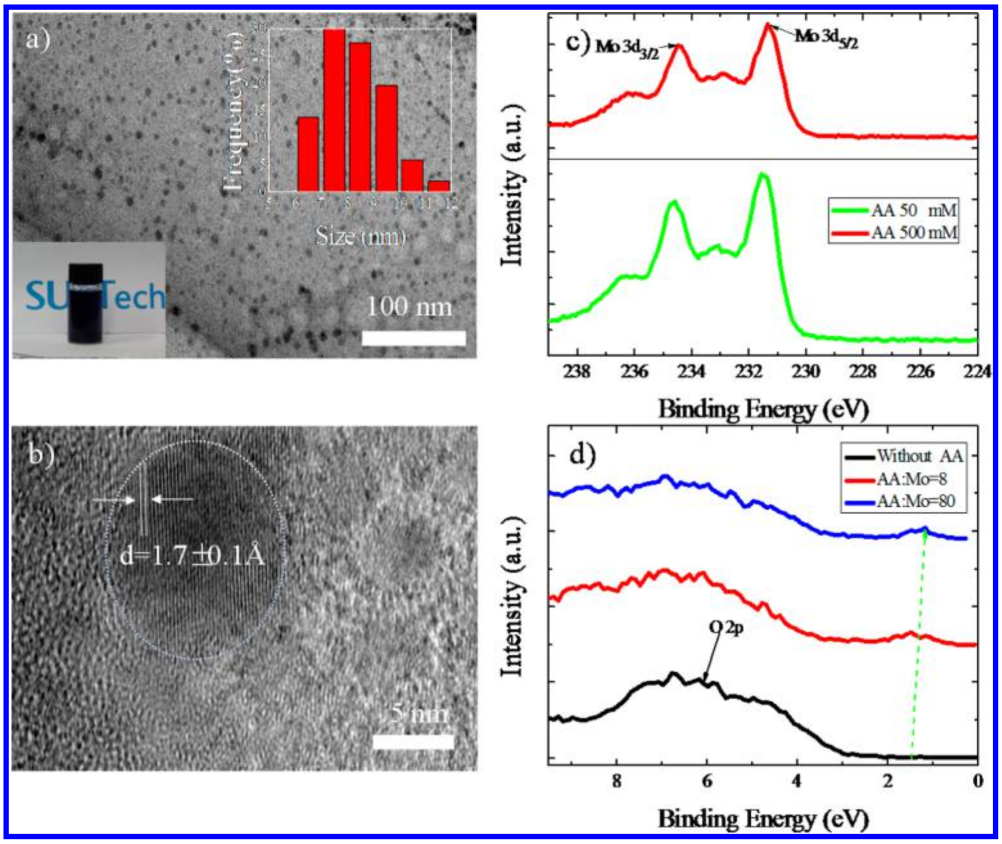

Figure 3. (a) TEM image of MoO_{3-x} nanodots with AA reduction (molar ratio of AA:Mo = 8). Inserted: photography of MoO_{3-x} solution. (b) HRTEM image for MoO_{3-x} nanodots with the same sample. Inserted: SAED pattern of MoO_{3-x} nanodots. (c) XPS spectra of Mo 3d and (d) O 2p of MoO_{3-x} with 8 and 80 molar ratio AA reduction.

nanodots are also overlapped by the Na element indicating that Na may also bond to molybdenum oxide nanodots.

Figure 2c shows the UV−vis absorption spectra of substoichiometry MoO_{3-x} nanodots with different $NaBH_4$ concentrations for the No. 2−8 samples. No. 9 was not conducted to test because of its rapid precipitation. The aggregation of colloids may be mainly attributed to the poor solubility of Mo(IV) oxide in aqueous solution. No. 2 showed no SPR peak at NIR region, while No. 3 and No. 4 exhibit a strong peak at 725 nm showing green color, and No. 5 and No. 6 with blue color exhibit a strong peak at 834 nm and a weak shoulder around 725 nm. Again, the brown No. 7 and No. 8 samples show no apparent absorption peak, which indicates no existed metallic phase. Meanwhile, no obvious plasmonic peak shift with various concentrations of reducing agents has been observed. From these results, it is concluded that the strong reductive capability of $NaBH_4$ induces fast crystal structure transformation instead of subtle carrier density adjustment; it is difficult to realize tunable plasmonic peak with the feasible reductant amount used.

Following this idea, weaker agents should be employed to investigate more detailed features of substoichiometry molybdenum oxides. It is well-known that AA is a much weaker reductant for mild reduction of metallic nanoparticles.[32] Therefore, it was employed to transform the as-prepared MoO_3 into substoichiometry nanodots. A 10 times higher dose of AA is considered compared to $NaBH_4$ because of the weaker reductive capability of organic acid, which the standard reduction potential of $NaBH_4$ in alkaline is −1.24 V but in AA is 0.13 V since it is 0.43 V for Mo(VI)/Mo(V).[32,33] The morphology characterization of substoichiometry MoO_{3-x} is shown in Figure 3a. The TEM image of AA reduction sample with molar ratio of AA:Mo = 6 exhibits a slightly smaller size compared with as-prepared MoO_3 nanodots. The average size distribution of nanodots is 8.26 ± 1.2 nm shown in the inserted image. Figure 3b also demonstrates the reductive substoichiometry MoO_{3-x} that shows similar crystal structure with pristine MoO_3 under HRTEM characterization. The lattice fringes show a spacing of 0.17 nm, which corresponds to the (123) plane of $MoO_{2.71}$. Comparing with the 0.18 nm pristine MoO_3 nanoparticles, the slight reduction in the *d*-spacing of reduced samples may be attributed to the presence of crystal lattice defects for ions vacancies.[19] The optical image also shows similar blue color against which mild reductive samples of $NaBH_4$ treatment are shown in the Figure 3a insert. To detect their valence state change, the XPS characterization (Figure 3c) has also been conducted with different AA reduction degree treatments. The molar ratio of AA:Mo is 8 and 80. The Mo 3d scanning spectra demonstrate that the Mo $3d_{3/2}$ doublet remains steady at 235.08 eV after increasing the amount of AA, and the Mo $3d_{5/2}$ doublet shifts slightly from 232.08 to 231.88 eV, suggesting that they possess the same substoichiometry in accordance with $MoO_{2.71}$ reductive state in the blue one prepared by $NaBH_4$ treatment, but no Mo(IV) could be observed under our experimental condition because of the weak reducing ability of AA. The slight peak shift may be as a result of abundant defects including molybdenum and oxygen vacancies. In addition, their O 2p scanning spectra in Figure 3d also show a weak peak at around 6.98 eV both in high and low AA reductant concentration comparing with as-prepared MoO_3. This peak is related to the fact that oxygen vacancies' electrons wave function overlaps with occupied Mo 4d states, indicating that the substoichiometry

DOI: 10.1021/acs.jpcc.6b11047
J. Phys. Chem. C 2017, 121, 5208−5214

oxides appear as a transformation from semiconductor to metallic behavior.[20] The EDX mapping shown in Figure 4 confirms the random distribution of MoO_{3-x} nanodots and no other impurity element observation besides Mo and O in the AA reducing sample.

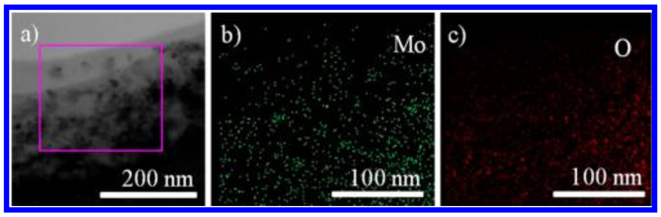

Figure 4. (a) STEM image of AA reducing MoO_{3-x} nanodots (molar ratio of AA:Mo = 8); (b) STEM EDX mapping of Mo and (c) O signals.

To study the plasmonic properties of MoO_{3-x} nanodots via AA reduction, the UV−vis−NIR absorption spectra were conducted for oxide nanodots with different reductant doses; the molar ratio of AA:Mo ranges from 6 to 136. The observed evident red-shift of SPR wavelength with the increment of AA concentration is shown in Figure 5b. With a small amount of AA (molar ratio = 6), oxides rendered SPR mode occurring at a wavelength of 830 nm, which is consistent with the blue sample prepared via mild $NaBH_4$ reduction. However, with addition of more AA reductant, the SPR energy of substoichiometry oxide nanodots gradually decreases. The molar ratio = 136 oxides showed a resonance peak at a wavelength of 872 nm. With higher AA concentration, a shoulder around 725 nm can be observed which is similar to the previous case by using $NaBH_4$ (Figure 2c). This peak can be ascribed to the absorption of remaining $MoO_{2.89}$ because of incomplete phase transformation. The relationship plot between AA concentration and SPR wavelength is shown in Figure 5c, which exhibits a nearly linear dependence of plasmonic shift versus reductant doses. According to eq 1, the carrier concentration can be obtained once the plasmon frequency is known. For reference, the calculated carrier concentrations for the samples under different AA treatments are around 5.89×10^{21} cm^{-3} (AA:Mo = 6), 5.86×10^{21} cm^{-3} (AA:Mo = 8), 5.74×10^{21} cm^{-3} (AA:Mo = 20), 5.67×10^{21} cm^{-3} (AA:Mo = 40), 5.55×10^{21} cm^{-3} (AA:Mo = 80), and 5.34×10^{21} cm^{-3} (AA: Mo = 136). The inserted image in Figure 5c is the near-field enhancements in the surface region of MoO_{3-x} nanodots. The calculation was performed by finite difference time domain (FDTD) simulations, which show the local electric field enhancement corresponding to the 850 nm wavelength with background refractive index of 1.33. A relatively high enhancement factor around 15 could be observed near the nanodot surface, making a promise for use in future sensing studies.

For the AA treatment, the samples do not show similar multiphase with the three color transition in $NaBH_4$ reduction but show only a single plasmonic absorption peak around 835 nm. Unlike $NaBH_4$, AA is a weak organic acid reductant, which could not result in alkali metal ion (Na^+) intercalation among the multilayer MoO_3 structure. For the partial reduction of Mo oxidation states, Na^+ intercalation would bring various color change with different reduction states of oxides (known as "molybdenum bronze")[34] and would expand them to other oxides such as V_2O_5, Nb_2O_5, and WO_3.[35] Therefore, the nonmetal ion AA reduction process displaying a clearly blue color with an 835 nm absorption peak produced a certain structure phase and stoichiometry. Similar SPR phenomena in ultrathin MoO_{3-x} nanosheets have been reported previously.[13]

The reason why weak organic acid reductant results in an evident shift of SPR wavelength may be primarily attributed to the surface defect states in the oxide nanodots under the same level of size distribution. For previous $Cu_{2-x}S$ nanocrystals, the redox reaction could control anion or cation vacancy concentration via introduction of chemical oxidant or reductant. According to semiconductor and plasmon frequency behavior, the higher

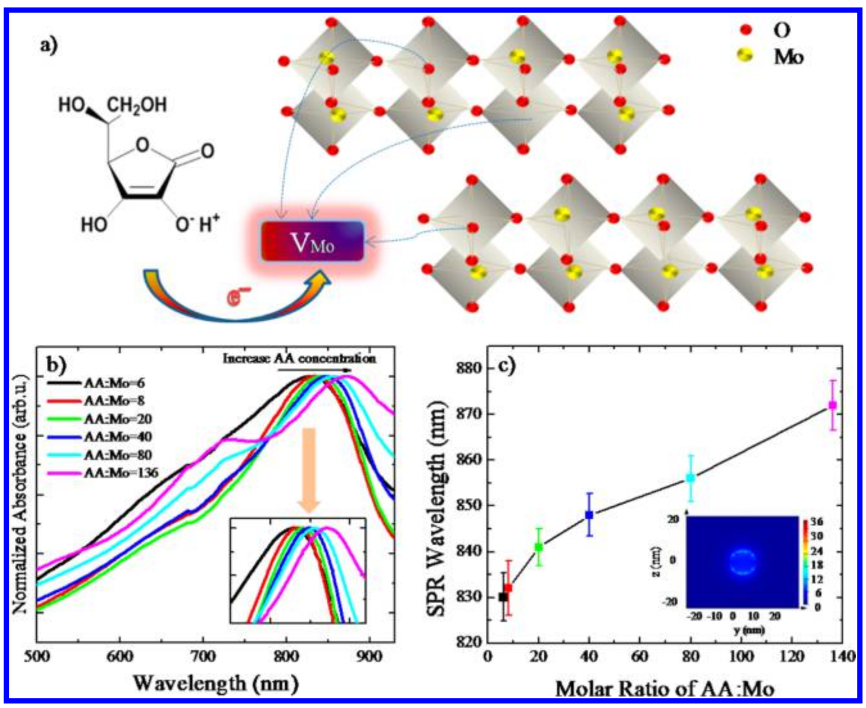

Figure 5. (a) Schematic diagram of AA reduction process for MoO_{3-x} defects. (b) UV−vis absorption spectra of MoO_{3-x} nanodots aqueous with various AA doses. (c) The corresponding response of oxide SPR peaks as a function of molar ratio of AA reductant/Mo source.

DOI: 10.1021/acs.jpcc.6b11047
J. Phys. Chem. C 2017, 121, 5208−5214

doping level brings more free carriers that could trigger higher plasmonic energy. The extraction of cation or anion is equal to leave behind a hole or an electron. Meanwhile, the ions vacancies could result in the increase of carrier concentration that leads to blue shifts of plasmonic resonance wavelength. In contrast, the interstice of cation or anion could bring a drop of carrier concentration leading to red shifts of plasmon energy.[18]

For the AA reduction procedure, organic acid in aqueous solution first produces protons via ionization. Subsequently, the ascorbate ions serving as the mild reducing agent would loss an electron to form a radical cation. The radical cation could still be oxidized to lose the second electron. It is speculated that there are numerous Mo vacancies existing on the surface of substoichiometry oxides, which result in p-type doping in semiconductor. The higher concentration of AA reductant could reverse to fill up vacancies because of the electron donor in reduction. The decrease of cation vacancies leads to red shift of plasmon energy through reduced free-carrier concentration. The schematic process is elucidated in Figure 5a. Besides the influence of cation vacancies, recent reports also found that this organic acid has the surface passivation effect to eliminate oxide surface defects. The protons provided by the organic acid could fill in the missing element space in the defect sites. This has been utilized for removing surface contaminants in two dimension MoS_2 monolayer, which significantly improves their photoluminescence efficiency.[36] Therefore, the protonation process may also be inevitable leading to the decrease of ion vacancies and free-carrier density.

The SPR peak position can be described by the refractive index of its environment by the following equation.

$$\lambda_{max} = \lambda_p \sqrt{1 + 2n_m^2} \tag{3}$$

where λ_{max} is the SPR peak wavelength. It can be seen that the corresponding wavelength is proportional to the refractive index of the surrounding medium. As a result, a longer SPR wavelength will be observed in a higher refractive index solvent. Figure 6a

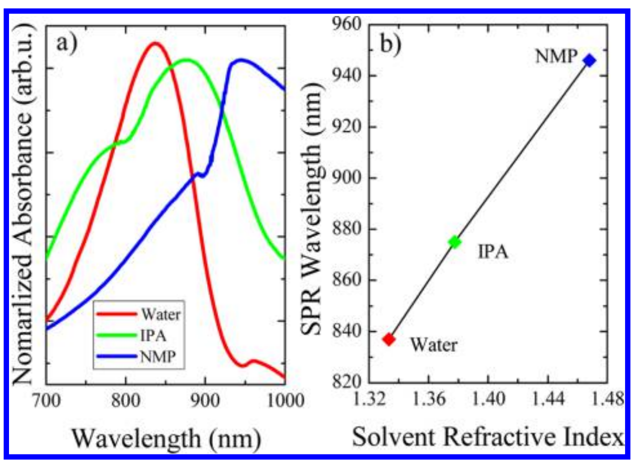

Figure 6. (a) SPR response of MoO_{3-x} nanodots in different solvents. (b) Observed SPR wavelength as a function of the refractive index of the solvents.

displays spectra of MoO_{3-x} nanodots in three different solvents undergoing molar ratio = 16 AA reduction, including deionized water, isopropyl alcohol (IPA), and *N*-methyl-2-pyrrolidone (NMP) with refractive indexes of 1.33, 1.38, and 1.47, respectively. The observed decrement of SPR peak energy with increasing refractive index of solvent is in accordance with the expected red-shift of plasmon peak, that is, 838 nm of the SPR peak in water and 946 nm of it in NMP. The shift of observed SPR wavelength is nearly 110 nm after changing the surrounding medium from water to NMP as shown in Figure 6b. It exhibits a high plasmonic sensitivity of 771 nm per refractive index unit (nm/RIU), which is higher than other plasmonic nanocrystals like WO_{3-x} (280 nm/RIU) and $Cu_{2-x}S$ (350 nm/RIU).[19] The improved sensitivity may be attributed to the extremely small nanodots with enhanced electric field intensity according to previous FDTD simulations. Similar with metallic nanoparticles and other plasmonic TMO counterparts, this result provides a platform to realize novel plasmonic semiconductors for refractive index sensing applications, such as detecting the dielectric constant of surrounding medium with high sensitivity

4. CONCLUSIONS

In summary, NIR plasmonic resonance of MoO_{3-x} nanodots has been prepared through a one-step reduction process in aqueous solution. Two different reductants have been utilized and compared to obtain various substoichiometry molybdenum oxides colloids, which showed much different optical responses. The $NaBH_4$ could result in a different substoichiometry oxide but with no SPR peak tunability once reduction finished. The AA reductive oxides realized dynamic tunability of plasmonic energy resonance through controlling their intrinsic carrier concentration as a result of defect alternation. With increasing interests of SPR behavior in semiconductors, the better understanding of plasmonic nanostructured MoO_{3-x} nanodots could provide a new platform to investigate their related applications, such as light harvesting, photothermal therapy, and sensing device.

■ ASSOCIATED CONTENT

Supporting Information

The Supporting Information is available free of charge on the ACS Publications website at DOI: 10.1021/acs.jpcc.6b11047.

Additional transmission electron microscopy images of pristine MoO_3 nanodots and EDX mappings for $NaBH_4$ reducing samples used in the present work (PDF)

■ AUTHOR INFORMATION

Corresponding Authors

*E-mail: tche@szu.edu.cn.
*E-mail: chen.r@sustc.edu.cn.
*E-mail: zktang@umac.mo.

ORCID

Rui Chen: 0000-0002-0445-7847

Notes

The authors declare no competing financial interest.

■ ACKNOWLEDGMENTS

This work is supported by the Natural Science Foundation of China (NSFC Grant Nos. 11574130, 11404161, and 11404219), Shenzhen Science and Technology Innovation Committee (Projects Nos.: JCYJ20150630162649956, JCYJ20150930160634263, and KQTD2015071710313656). R. C. acknowledges the support from national 1000 plan for young talents.

■ REFERENCES

(1) Link, S.; Mohamed, M. B.; El-Sayed, M. A. Simulation of the Optical Absorption Spectra of Gold Nanorods as a Function of Their

Aspect Ratio and the Effect of the Medium Dielectric Constant. *J. Phys. Chem. B* **1999**, *103*, 3073−3077.

(2) Cheng, C. W.; Sie, E. J.; Liu, B.; Huan, C. H. A.; Sum, T. C.; Sun, H. D.; Fan, H. J. Surface Plasmon Enhanced Band Edge Luminescence of ZnO Nanorods by Capping Au Nanoparticles. *Appl. Phys. Lett.* **2010**, *96*, 071107.

(3) Sanz-Ortiz, M. N.; Sentosun, K.; Bals, S.; Liz-Marzán, L. M. Templated Growth of Surface Enhanced Raman Scattering-Active Branched Gold Nanoparticles within Radial Mesoporous Silica Shells. *ACS Nano* **2015**, *9*, 10489−10497.

(4) Jain, P. K.; Huang, X.; El-Sayed, I. H.; El-Sayed, M. A. Review of Some Interesting Surface Plasmon Resonance-Enhanced Properties of Noble Metal Nanoparticles and Their Applications to Biosystems. *Plasmonics* **2007**, *2*, 107−118.

(5) Sobhani, A.; Manjavacas, A.; Cao, Y.; McClain, M. J.; García de Abajo, F. J.; Nordlander, P.; Halas, N. J. Pronounced Linewidth Narrowing of an Aluminum Nanoparticle Plasmon Resonance by Interaction with an Aluminum Metallic Film. *Nano Lett.* **2015**, *15*, 6946−6951.

(6) Luther, J. M.; Jain, P. K.; Ewers, T.; Alivisatos, A. P. Localized Surface Plasmon Resonances Arising from Free Carriers in Doped Quantum Dots. *Nat. Mater.* **2011**, *10*, 361−366.

(7) Zhao, Y.; Pan, H.; Lou, Y.; Qiu, X.; Zhu, J.; Burda, C. Plasmonic $Cu_{2-X}S$ Nanocrystals: Optical and Structural Properties of Copper-Deficient Copper(I) Sulfides. *J. Am. Chem. Soc.* **2009**, *131*, 4253−4261.

(8) Faucheaux, J. A.; Stanton, A. L. D.; Jain, P. K. Plasmon Resonances of Semiconductor Nanocrystals: Physical Principles and New Opportunities. *J. Phys. Chem. Lett.* **2014**, *5*, 976−985.

(9) Jain, P. K.; Manthiram, K.; Engel, J. H.; White, S. L.; Faucheaux, J. A.; Alivisatos, A. P. Doped Nanocrystals as Plasmonic Probes of Redox Chemistry. *Angew. Chem., Int. Ed.* **2013**, *52*, 13671−13675.

(10) Schimpf, A. M.; Knowles, K. E.; Carroll, G. M.; Gamelin, D. R. Electronic Doping and Redox-Potential Tuning in Colloidal Semiconductor Nanocrystals. *Acc. Chem. Res.* **2015**, *48*, 1929−1937.

(11) Garcia, G.; Buonsanti, R.; Runnerstrom, E. L.; Mendelsberg, R. J.; Llordes, A.; Anders, A.; Richardson, T. J.; Milliron, D. J. Dynamically Modulating the Surface Plasmon Resonance of Doped Semiconductor Nanocrystals. *Nano Lett.* **2011**, *11*, 4415−4420.

(12) Polking, M. J.; Jain, P. K.; Bekenstein, Y.; Banin, U.; Millo, O.; Ramesh, R.; Alivisatos, A. P. Controlling Localized Surface Plasmon Resonances in GeTe Nanoparticles Using an Amorphous-to-Crystalline Phase Transition. *Phys. Rev. Lett.* **2013**, *111*, 037401.

(13) Manthiram, K.; Alivisatos, A. P. Tunable Localized Surface Plasmon Resonances in Tungsten Oxide Nanocrystals. *J. Am. Chem. Soc.* **2012**, *134*, 3995−3998.

(14) Buonsanti, R.; Llordes, A.; Aloni, S.; Helms, B. A.; Milliron, D. J. Tunable Infrared Absorption and Visible Transparency of Colloidal Aluminum-Doped Zinc Oxide Nanocrystals. *Nano Lett.* **2011**, *11*, 4706−4710.

(15) Faucheaux, J. A.; Jain, P. K. Plasmons in Photocharged ZnO Nanocrystals Revealing the Nature of Charge Dynamics. *J. Phys. Chem. Lett.* **2013**, *4*, 3024−3030.

(16) Kim, J.; Agrawal, A.; Krieg, F.; Bergerud, A.; Milliron, D. J. The Interplay of Shape and Crystalline Anisotropies in Plasmonic Semiconductor Nanocrystals. *Nano Lett.* **2016**, *16*, 3879−84.

(17) Runnerstrom, E. L.; Bergerud, A.; Agrawal, A.; Johns, R. W.; Dahlman, C. J.; Singh, A.; Selbach, S. M.; Milliron, D. J. Defect Engineering in Plasmonic Metal Oxide Nanocrystals. *Nano Lett.* **2016**, *16*, 3390−3398.

(18) Alsaif, M. M. Y. A.; Field, M. R.; Daeneke, T.; Chrimes, A. F.; Zhang, W.; Carey, B. J.; Berean, K. J.; Walia, S.; van Embden, J.; Zhang, B.; et al. Exfoliation Solvent Dependent Plasmon Resonances in Two-Dimensional Sub-Stoichiometric Molybdenum Oxide Nanoflakes. *ACS Appl. Mater. Interfaces* **2016**, *8*, 3482−3493.

(19) Mattox, T. M.; Ye, X.; Manthiram, K.; Schuck, P. J.; Alivisatos, A. P.; Urban, J. J. Chemical Control of Plasmons in Metal Chalcogenide and Metal Oxide Nanostructures. *Adv. Mater.* **2015**, *27*, 5830−5837.

(20) Alsaif, M. M. Y. A.; Latham, K.; Field, M. R.; Yao, D. D.; Medehkar, N. V.; Beane, G. A.; Kaner, R. B.; Russo, S. P.; Ou, J. Z.; Kalantar-zadeh, K. Tunable Plasmon Resonances in Two-Dimensional Molybdenum Oxide Nanoflakes. *Adv. Mater.* **2014**, *26*, 3931−3937.

(21) Huang, Q.; Hu, S.; Zhuang, J.; Wang, X. MoO_{3-x}-Based Hybrids with Tunable Localized Surface Plasmon Resonances: Chemical Oxidation Driving Transformation from Ultrathin Nanosheets to Nanotubes. *Chem. - Eur. J.* **2012**, *18*, 15283−15287.

(22) Cheng, H.; Qian, X.; Kuwahara, Y.; Mori, K.; Yamashita, H. A Plasmonic Molybdenum Oxide Hybrid with Reversible Tunability for Visible-Light-Enhanced Catalytic Reactions. *Adv. Mater.* **2015**, *27*, 4616−4621.

(23) Bao, T.; Yin, W.; Zheng, X.; Zhang, X.; Yu, J.; Dong, X.; Yong, Y.; Gao, F.; Yan, L.; Gu, Z.; et al. One-Pot Synthesis of Pegylated Plasmonic MoO_{3-x} Hollow Nanospheres for Photoacoustic Imaging Guided Chemo-Photothermal Combinational Therapy of Cancer. *Biomaterials* **2016**, *76*, 11−24.

(24) Alsaif, M. M. Y. A.; Field, M. R.; Murdoch, B. J.; Daeneke, T.; Latham, K.; Chrimes, A. F.; Zoolfakar, A. S.; Russo, S. P.; Ou, J. Z.; Kalantar-zadeh, K. Substoichiometric Two-Dimensional Molybdenum Oxide Flakes: A Plasmonic Gas Sensing Platform. *Nanoscale* **2014**, *6*, 12780−12791.

(25) Runnerstrom, E. L.; Llordes, A.; Lounis, S. D.; Milliron, D. J. Nanostructured Electrochromic Smart Windows: Traditional Materials and Nir-Selective Plasmonic Nanocrystals. *Chem. Commun.* **2014**, *50*, 10555−10572.

(26) Llordes, A.; Garcia, G.; Gazquez, J.; Milliron, D. J. Tunable Near-Infrared and Visible-Light Transmittance in Nanocrystal-in-Glass Composites. *Nature* **2013**, *500*, 323−326.

(27) Qiu, J.; Wei, W. D. Surface Plasmon-Mediated Photothermal Chemistry. *J. Phys. Chem. C* **2014**, *118*, 20735−20749.

(28) Atwater, H. A.; Polman, A. Plasmonics for Improved Photovoltaic Devices. *Nat. Mater.* **2010**, *9*, 205−213.

(29) Smith, J. G.; Faucheaux, J. A.; Jain, P. K. Plasmon Resonances for Solar Energy Harvesting: A Mechanistic Outlook. *Nano Today* **2015**, *10*, 67−80.

(30) Mayer, K. M.; Hafner, J. H. Localized Surface Plasmon Resonance Sensors. *Chem. Rev.* **2011**, *111*, 3828−3857.

(31) Dong, L.; Lin, S.; Yang, L.; Zhang, J.; Yang, C.; Yang, D.; Lu, H. Spontaneous Exfoliation and Tailoring of MoS_2 in Mixed Solvents. *Chem. Commun.* **2014**, *50*, 15936−15939.

(32) Jana, N. R.; Gearheart, L.; Murphy, C. J. Seeding Growth for Size Control of 5−40 Nm Diameter Gold Nanoparticles. *Langmuir* **2001**, *17*, 6782−6786.

(33) Schaeffer, G. W.; Waller, M. C.; Hohnstedt, L. F. Aqueous Sodium Borohydride Chemistry. Lead, Barium, Mercury, Cadmium, and Zinc. *Anal. Chem.* **1961**, *33*, 1719−1722.

(34) Greenblatt, M. Molybdenum Oxide Bronzes with Quasi-Low-Dimensional Properties. *Chem. Rev.* **1988**, *88*, 31−53.

(35) Kalantar-zadeh, K.; Ou, J. Z.; Daeneke, T.; Mitchell, A.; Sasaki, T.; Fuhrer, M. S. Two Dimensional and Layered Transition Metal Oxides. *Appl. Mater. Today* **2016**, *5*, 73−89.

(36) Amani, M.; Lien, D. H.; Kiriya, D.; Xiao, J.; Azcatl, A.; Noh, J.; Madhvapathy, S. R.; Addou, R.; KC, S.; Dubey, M.; et al. Near-Unity Photoluminescence Quantum Yield in MoS_2. *Science* **2015**, *350*, 1065−1068.

DOI: 10.1021/acs.jpcc.6b11047
J. Phys. Chem. C 2017, 121, 5208−5214